JOURNAL OF MATERIALS SCIENCE 32 (1997) 2797–2809

Modelling concurrent deformation mechanisms in auxetic microporous polymers

A. ALDERSON*, K. E. EVANS
School of Engineering, University of Exeter, North Park Road, Exeter EX4 4QF, UK

A 2D model for the deformation of auxetic microporous polymers (those with a negative Poisson's ratio) has been previously developed, consisting of a network of rigid rectangular nodules interconnected by fibrils. This model has now been extended to describe the deformation of the network via concurrent fibril hinging and stretching mechanisms. Expressions for the strain-dependent Poisson's ratios and Young's moduli are derived and fully investigated with respect to their dependence on the model parameters. These expressions are compared with the experimental strain-dependent data for auxetic microporous polytetrafluoroethylene (PTFE) and ultra-high molecular weight polyethylene (UHMWPE). The use of concurrent deformation mechanisms makes a very significant improvement in the agreement of theory with experiment for both cases. Slight discrepancies are discussed in terms of the use of the assumptions of a 2D network of regular, rectangular nodules and a constant force coefficient ratio governing the two deformation mechanisms.

1. Introduction

In recent years materials have been fabricated that have the novel property of a negative Poisson's ratio, i.e. they expand laterally when stretched longitudinally. Such materials, known as *auxetic materials* [1], generally exhibit a negative Poisson's ratio due to the geometry and deformation mechanisms of, for example, the microstructure in microporous polymers [2–4] or on a larger scale in auxetic foams [5, 6]. Auxetic behaviour has also been observed in the naturally occurring mineral α-cristobalite [7] where the deformation mechanism acts on a molecular scale [7, 8]. As well as obvious applications for auxetic materials as, for example, fasteners and seals, the property of a negative Poisson's ratio can lead to improved mechanical properties such as increased fracture toughness and enhanced indentation resistance [5, 9, 10].

In the case of microporous polymers, expanded forms of polytetrafluoroethylene (PTFE) [2], ultra-high molecular weight polyethylene (UHMWPE) [11, 12] and polypropylene [13] have been fabricated and observed to be auxetic. The microstructure producing the negative Poisson's ratio in these polymeric materials consists of a network of nodules interconnected by fibrils. A simple geometric node–fibril (NF) model has been developed [11, 12, 14] where a regular array of rigid square or rectangular nodules is formed into a connected network by freely hinged inextensible rods (fibrils). Deformation of the network is by hinging of the fibrils in response to an applied load and can result in positive and negative strain-dependent Poisson's ratios, depending entirely on the geometry of the network. The model has recently been extended to include flexure and stretching of the fibrils [15]. A combination of fibril hinging followed by fibril stretching has been found to explain all the general features of the experimental data. However, in reality, fibril hinging and stretching will occur concurrently rather than consecutively. In this paper we develop the NF model to include simultaneous fibril hinging and stretching. The strain-dependent elastic moduli calculated from the concurrent model are then compared with the experimental data for PTFE and UHMWPE.

2. Concurrent node–fibril model

The tensile NF network model for microporous polymers is shown schematically in Fig. 1a, consisting of a regular array of rigid rectangular nodules (major axis length a and minor axis length b aligned along the x and y axes, respectively) interconnected by hinged rods (fibrils) of length l at an angle α to the x axis. If we assume that shear deformation of the fibrils can be neglected (valid for all fibril aspect ratios so far observed [2, 4]) then the network can deform by hinging, flexure and stretching of the fibrils. Elastic moduli due to each of these modes of deformation have been derived in an earlier paper by the authors [15]. Experimentally, no evidence for fibril flexure has been observed and the current model fails to describe the strain dependence of the elastic properties with sufficient accuracy throughout the strain range. We, therefore, now obtain expressions for Poisson's ratios and

* Permanent address: BNFL, Company Research Laboratory, B516, Springfields, Preston, Lancashire PR4 0XJ, UK

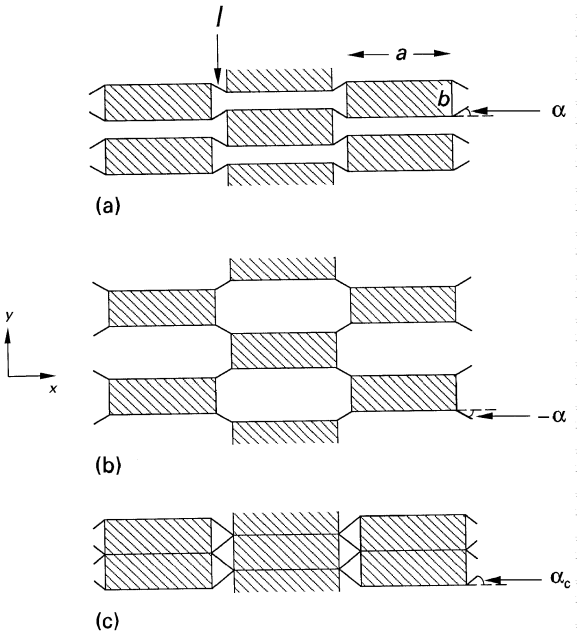

Figure 1 (a) Schematic diagram of the nodule–fibril (NF) model, showing the general parameters in a partially extended network. (b) The NF model microstructure with a negative fibril angle α. (c) The NF model microstructure with $l > b/2$ and nodules in contact in the y direction.

Young's moduli due to fibril hinging and stretching acting concurrently.

The repeat unit-cell lengths X and Y in the x and y directions, respectively, of Fig. 1 are given by

$$X = 2(a + l\cos\alpha) \tag{1}$$

$$Y = 2(b - l\sin\alpha) \tag{2}$$

Consider, first, a change $\Delta\sigma_x$ in an applied stress in the x direction. It has been shown [15] that the changes in the unit-cell lengths due to hinging are

$$\Delta X_h = \Delta\sigma_x Y l^2 \sin^2\alpha/K_h \tag{3}$$

$$\Delta Y_h = \Delta\sigma_x Y l^2 \sin\alpha\cos\alpha/K_h \tag{4}$$

K_h is the hinging force coefficient defined by

$$K_h = \Delta M/\Delta\alpha \tag{5}$$

where ΔM is the change in the applied moment to the fibril due to the change in applied stress, and $\Delta\alpha$ is the angular displacement of the fibril due to ΔM.

Similarly, it has been shown [15] that the changes in the unit-cell lengths due to fibril stretching are in this case

$$\Delta X_s = \Delta\sigma_x Y\cos^2\alpha/K_s \tag{6}$$

$$\Delta Y_s = -\Delta\sigma_x Y\sin\alpha\cos\alpha/K_s \tag{7}$$

The stretching force coefficient K_s is defined by

$$K_s = \Delta F/\Delta s \tag{8}$$

where ΔF is the change in force applied along the length of the fibril due to $\Delta\sigma_x$, and Δs is the change in extension of the fibril due to ΔF.

For an infinitesimal change in applied load ($\Delta\sigma_x \to d\sigma_x$), the total changes in X and Y due to fibril hinging and stretching acting concurrently are simply

$$dX_{tot} = dX_h + dX_s \tag{9}$$

$$dY_{tot} = dY_h + dY_s \tag{10}$$

The Poisson's ratio ν_{xy} due to an infinitesimal change in the applied uniaxial stress along the x axis at any instant during non-linear elastic deformation is defined by the tangent Poisson's ratio (or Poisson's function) [15–17]

$$\nu_{xy} = -d\varepsilon_y/d\varepsilon_x \tag{11}$$

where $d\varepsilon_x$ and $d\varepsilon_y$ are the infinitesimal changes in strain in the x and y directions, respectively, given by

$$d\varepsilon_x = dX/X \tag{12}$$

$$d\varepsilon_y = dY/Y \tag{13}$$

Hence from Equations 1–4, 6, 7 and 9–13 we have

$$\nu_{xy} = \frac{[1 - (l^2K_s/K_h)]\sin\alpha\cos\alpha\,(a + l\cos\alpha)}{[(l^2K_s/K_h)\sin^2\alpha + \cos^2\alpha]\,(b - l\sin\alpha)} \tag{14}$$

Similarly, defining the strain-dependent Young's modulus during non-linear deformation as the tangent modulus [15, 18] at a given strain we have for an x-directed load

$$E_x = d\sigma_x/d\varepsilon_x \tag{15}$$

From Equations 1–3, 6, 9, 12 and 15 we have, therefore

$$E_x = \frac{a + l\cos\alpha}{(b - l\sin\alpha)[(l^2\sin^2\alpha/K_h) + (\cos^2\alpha/K_s)]} \tag{16}$$

Experimentally it is the engineering Young's modulus E_x^e that is often measured in tensile tests. The model expression for E_x^e is found by substituting the initial undeformed unit-cell lengths X_0 and Y_0 for X and Y, respectively, in Equations 3, 6 and 12, giving

$$E_x^e = \frac{a + l_0\cos\alpha_0}{(b - l_0\sin\alpha_0)[(l^2\sin^2\alpha/K_h) + (\cos^2\alpha/K_s)]} \tag{17}$$

where l_0 and α_0 are the initial fibril length and angle, respectively.

For completeness, we derive the engineering Poisson's ratio by substituting X_0 and Y_0 for X and Y in Equations 12 and 13, respectively, to be

$$\nu_{xy}^e = \frac{[1 - (l^2K_s/K_h)]\sin\alpha\cos\alpha\,(a + l_0\cos\alpha_0)}{[(l^2K_s/K_h)\sin^2\alpha + \cos^2\alpha]\,(b - l_0\sin\alpha_0)} \tag{18}$$

Now consider a uniaxial stress σ_y applied in the y direction. In this case the changes in the unit-cell lengths due to fibril hinging in response to a change $\Delta\sigma_y$ in the applied stress have been shown [15] to be

$$\Delta X_h = \Delta\sigma_y X l^2\sin\alpha\cos\alpha/K_h \tag{19}$$

$$\Delta Y_h = \Delta\sigma_y X l^2\cos^2\alpha/K_h \tag{20}$$

and due to fibril stretching

$$\Delta X_s = -\Delta\sigma_y X \sin\alpha\cos\alpha/K_s \quad (21)$$

$$\Delta Y_s = \Delta\sigma_y X \sin^2\alpha/K_s \quad (22)$$

Following a similar procedure to that used above for an x-directed load we find in the case of a y-directed load

$$\nu_{yx} = \frac{[1-(l^2K_s/K_h)]\sin\alpha\cos\alpha}{[(l^2K_s/K_h)\cos^2\alpha+\sin^2\alpha]}\frac{b-l\sin\alpha}{a+l\cos\alpha} \quad (23)$$

$$\nu^e_{yx} = \frac{[1-(l^2K_s/K_h)]\sin\alpha\cos\alpha}{[(l^2K_s/K_h)\cos^2\alpha+\sin^2\alpha]}\frac{b-l_0\sin\alpha_0}{a+l_0\cos\alpha_0} \quad (24)$$

$$E_y = \frac{b-l\sin\alpha}{(a+l\cos\alpha)[(l^2\cos^2\alpha/K_h)+(\sin^2\alpha/K_s)]} \quad (25)$$

$$E^e_y = \frac{b-l_0\sin\alpha_0}{(a+l_0\cos\alpha_0)[(l^2\cos^2\alpha/K_h)+(\sin^2\alpha/K_s)]} \quad (26)$$

All these expressions are equally valid in tension or compression.

For an orthotropic material a symmetric stiffness matrix implies [19]

$$\nu_{xy}E_y = \nu_{yx}E_x \quad (27)$$

and the requirement of a positive definite strain energy for static equilibrium leads to the condition [19]

$$|\nu_{xy}| \leqslant (E_x/E_y)^{1/2} \quad (28)$$

It is easily verified that Equations 14, 16, 23 and 25 satisfy Equations 27 and 28. Furthermore, setting either K_s or K_h equal to infinity reduces the expressions to those due to hinging and stretching, respectively [15].

3. Results

In this section the trends of the elastic moduli for the NF model employing concurrent fibril hinging and stretching are considered in response to varying the geometric and force coefficient parameters in the model. Strain-history behaviour from a pre-defined undeformed geometry is then considered and comparison is made with the experimental strain-dependent data for auxetic PTFE [2] and UHMWPE [12, 16].

3.1. Effect of varying the model parameters on the elastic moduli

For convenience we define an effective hinging force coefficient K_h^{eff} as

$$K_h^{eff} = K_h/l^2 \quad (29)$$

The elastic moduli were calculated for an arbitrary initial standard parameter set of $b/a = 1$, $l = 0.25a$, $l_0 = 0.25a$, $K_s/K_h^{eff} = 10$, $\alpha = 45^\circ$ and $\alpha_0 = 45^\circ$. The effect of varying any one parameter on the behaviour of the elastic moduli while keeping the others constant was examined.

The effect of varying the force coefficients ratio, K_s/K_h^{eff}, is shown in Figs 2 and 3 for the Poisson's ratio and Young's modulus, respectively, due to loading in the x direction. ν_{xy} was calculated from Equation 14 and E_x was calculated from Equation 16. Curves for each of the elastic moduli versus α are shown for $K_s/K_h^{eff} = 0.01$, 0.1, 1, 10 and 100 with all other parameters as standard. Also shown are the curves due to hinging and stretching acting independently (i.e. K_s and K_h infinite, respectively).

From Fig. 2 ν_{xy} is seen to be zero at $\alpha = 0^\circ$ for deformation due solely to fibril stretching. As α increases ν_{xy} becomes positive, increasing to infinity as α tends to 90°, due to the absence of an x-directed stress along the length of the fibril when $\alpha = 90^\circ$. Fibril hinging shows markedly different behaviour, exhibiting an infinitely negative ν_{xy} at $\alpha = 0^\circ$ (i.e. there is no component of an x-directed stress perpendicular to the fibril with which to cause hinging when $\alpha = 0^\circ$), which decreases in magnitude to $\nu_{xy} = 0$ at $\alpha = 90^\circ$.

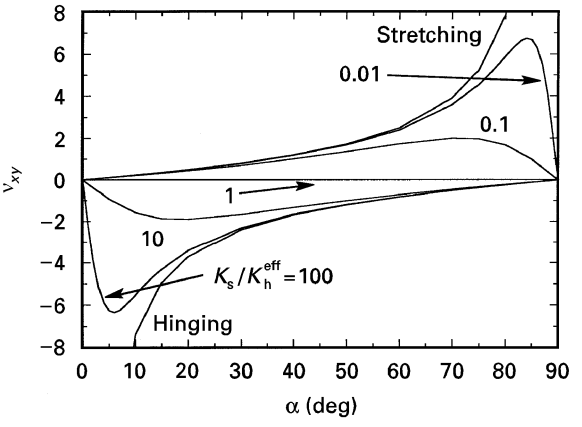

Figure 2 ν_{xy} versus α for the NF model employing concurrent fibril hinging and stretching mechanisms. Curves are for $K_s/K_h^{eff} = 0.01$, 0.1, 1, 10, 100 and stretching and hinging mechanisms acting independently. Calculations were performed with $b/a = 1$ and $l = 0.25a$.

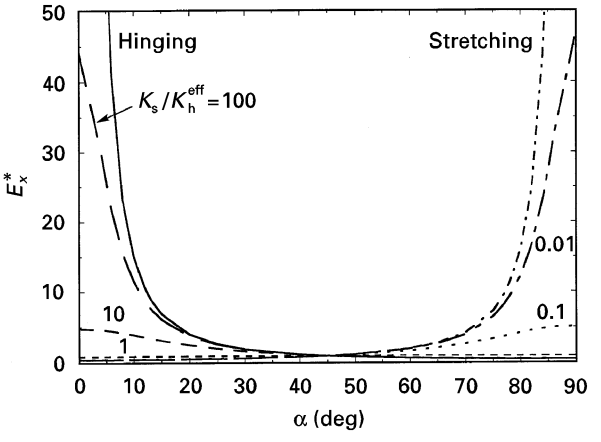

Figure 3 Normalized Young's modulus data E_x^* versus α for the NF model employing concurrent fibril hinging and stretching mechanisms. Curves are for $K_s/K_h^{eff} = 0.01$, 0.1, 1, 10, 100 and stretching and hinging mechanisms acting independently. Calculations were performed with $b/a = 1$ and $l = 0.25a$. For each curve the data are normalized to the calculated value at $\alpha = 45^\circ$, i.e. $E_x^* = E_x/E_x$ ($\alpha = 45^\circ$).

Hence for $0 < \alpha < 90^\circ$ fibril stretching results in a positive ν_{xy}, whereas fibril hinging leads to a negative ν_{xy}. For intermediate cases when K_s/K_h^{eff} is finite, $\nu_{xy} = 0$ at both $\alpha = 0$ and 90°. For $K_s/K_h^{eff} = 0.01$ stretching dominates, with ν_{xy} remaining positive for $0 < \alpha < 90^\circ$. In fact, for $0 < \alpha < 70^\circ$ the ν_{xy} curves for $K_s/K_h^{eff} = 0.01$ and 0 (stretching only) are almost identical. The maximum value of ν_{xy} for $K_s/K_h^{eff} = 0.01$ is $\nu_{xy} = 6.7$ and occurs for $\alpha \sim 84^\circ$, whereupon hinging becomes increasingly significant for further increases in α, as illustrated by the ν_{xy} curve tending towards the hinging curve for $84 < \alpha \leqslant 90^\circ$.

Increasing K_s/K_h^{eff} to 0.1 also results in a positive ν_{xy} for $0 < \alpha < 90^\circ$. However, the curve deviates significantly from that due to stretching only at a lower value of α ($\sim 50^\circ$) than the curve for $K_s/K_h^{eff} = 0.01$. The maximum value of ν_{xy} is also reduced to $\nu_{xy} \sim 2$ for $K_s/K_h^{eff} = 0.01$ which occurs at $\alpha \sim 70^\circ$ compared to the maximum of $\nu_{xy} = 6.7$ at $\alpha \sim 84^\circ$ for $K_s/K_h^{eff} = 0.01$.

When $K_s/K_h^{eff} = 1$, $\nu_{xy} = 0$ for all values of α. In other words, in this case neither hinging nor stretching dominates, leading to a cancellation of their macroscopic effects. Bearing in mind the definition of K_h^{eff} (Equation 29) and the form of K_s (see Section 4.1), this ratio is crucially dependent on the dimensions of the fibrils.

The curves for $K_s/K_h^{eff} = 10$ and 100 both exhibit negative ν_{xy} values for $0 < \alpha < 90^\circ$, indicating that hinging is the dominant mechanism in these cases, with the curve for $K_s/K_h^{eff} = 100$ lying closest to the curve due to hinging only. Hence the value of K_s/K_h^{eff} plays a critical role in determining both the magnitude and sign of ν_{xy} at any given fibril angle α.

The behaviour of ν_{yx} with α is similar but antisymmetric to the ν_{xy} trends, e.g. at $\alpha = 0^\circ$ $\nu_{yx} = +\infty$ (c.f. $\nu_{xy} = 0$) and at $\alpha = 90^\circ$ $\nu_{yx} = 0$ (c.f. $\nu_{xy} = +\infty$) when deformation is due to fibril stretching.

Since the expressions for the Young's moduli require absolute values of the two force coefficients, rather than simply the ratio, the Young's moduli data were normalized to the data calculated at $\alpha = 45^\circ$, i.e. $E_x^* = E_x/E_x(\alpha = 45^\circ)$. This choice of normalization angle was chosen because at $\alpha = 45^\circ$ the Young's modulus due to hinging is equal to that due to stretching when $K_s = K_h^{eff}$.

The value of E_x^* due to fibril stretching has a relatively low finite value ($E_x^* = 0.437$) at $\alpha = 0^\circ$ which slowly increases as α increases until α approaches 90°, whereupon E_x^* rapidly tends to infinity (due to the fibril being aligned normal to the loading direction at $\alpha = 90^\circ$) – see Fig. 3. Conversely, at $\alpha = 0^\circ$ E_x^* due to fibril hinging is infinite, decreasing rapidly as α increases before tailing off to $E_x^* = 0.466$ at $\alpha = 90^\circ$. As before, when $K_s/K_h^{eff} \ll 1$ stretching dominates and hence the E_x^* curve for $K_s/K_h^{eff} = 0.01$ lies closest to the stretching limit. However, even at this low value of K_s/K_h^{eff} the influence of hinging is such that at $\alpha = 90^\circ$ the modulus has a finite value as opposed to an infinite value for pure fibril stretching. For $K_s/K_h^{eff} = 0.1$ the E_x^* curve follows the same general trend as that for $K_s/K_h^{eff} = 0.01$. However, the curve for $K_s/K_h^{eff} = 0.1$ is much flatter, achieving a maximum value of only $E_x^* = 5.13$ at $\alpha = 90^\circ$ compared with $E_x^* = 47.10$ for $K_s/K_h^{eff} = 0.01$. When $K_s = K_h^{eff}$, E_x^* is approximately constant with α, deviating from unity by a maximum of $\sim 12\%$ (at $\alpha = 0^\circ$). For $K_s/K_h^{eff} \gg 1$ the E_x^* curve tends towards the hinging limit, although even at the highest K_s/K_h^{eff} ratios the influence of stretching constrains E_x^* to remain finite at $\alpha = 0^\circ$ as opposed to infinity for hinging only.

In the case of a y-directed load the Young's modulus trends are reversed, e.g. for deformation due to fibril stretching E_y^* is infinite at $\alpha = 0^\circ$ (c.f. $E_x^* =$ low and finite), rapidly decreasing as α increases before tailing off to a relatively low finite value at $\alpha = 90^\circ$ ($E_y^* = 0.536$ c.f. $E_x^* = \infty$).

The effect of varying the geometrical parameters in the model is illustrated in Fig. 4. For brevity only ν_{xy} behaviour is shown.

In Fig. 4a the ν_{xy} versus l behaviour is shown, with all other parameters defined as standard. Varying the fibril length is seen to alter the magnitude but not the sign of ν_{xy}, with the negative value of ν_{xy} increasing as l increases.

Fig. 4b shows the effect of varying the nodule aspect ratio on ν_{xy}, with all other parameters as standard. Once again the sign of ν_{xy} is independent of the aspect ratio, whereas the magnitude increases as b/a decreases.

Finally, Fig. 4c illustrates the behaviour of ν_{xy} with α in the range $-90 \leqslant \alpha \leqslant 90^\circ$, with all other parameters as standard. This range of α includes negative values of the fibril angle which have not been considered hitherto in this paper. An example of the NF model microstructure with α negative is shown schematically in Fig. 1b. It is seen from Fig. 4c that the sign of α is also critical in determining the sign of ν_{xy}. For the standard model parameters used in the calculations for Fig. 4c positive and negative values of α yield negative and positive ν_{xy} values, respectively. As already noted the magnitude of ν_{xy} also varies with α.

To summarize this section, we have seen that the elastic moduli are determined by both the geometry and force coefficients involved in the deformation of the network microstructure.

3.2. Calculation of strain in the concurrent NF model

In order to compare the NF model to the experimental data for PTFE [2] and UHMWPE [12, 16] it is necessary to calculate the elastic moduli as functions of the total true strain in the loading direction. This requires both a knowledge of the initial undeformed geometry of the NF microstructure and how the fibril length varies with fibril angle as the microstructure deforms. Following ref. [15], we have calculated the total true strain in the x direction by integrating the infinitesimal increment of true strain defined by Equation 12, i.e.

$$\varepsilon_x = \int_{X_0}^{X} dX/X = \ln(X/X_0) \qquad (30)$$

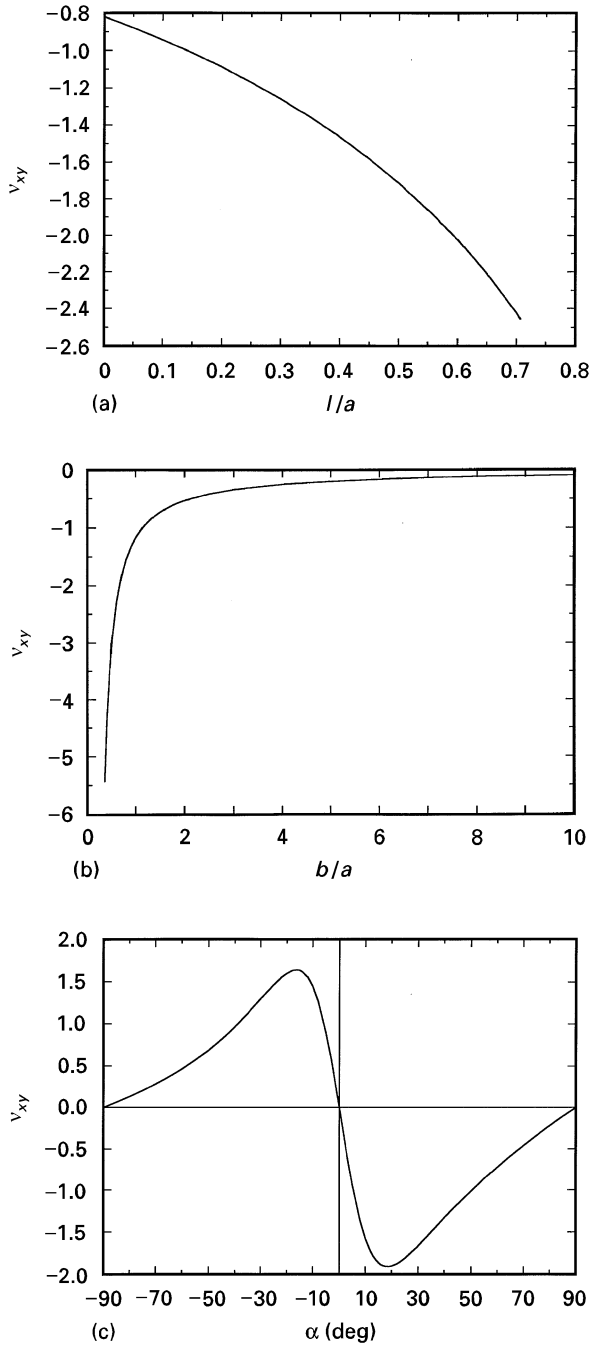

Figure 4 ν_{xy} trends for the NF model employing concurrent fibril hinging and stretching mechanisms calculated for a standard parameter set of $b/a = 1$, $K_s/K_h^{eff} = 10$, $l = 0.25a$ and $\alpha = 45°$. (a) ν_{xy} versus l/a; (b) ν_{xy} versus b/a; (c) ν_{xy} versus α.

Substituting Equation 1 into Equation 30 yields

$$\varepsilon_x = \ln[(a + l\cos\alpha)/(a + l_0\cos\alpha_0)] \tag{31}$$

where l_0 and α_0 are the initial fibril length and angle, respectively.

Similarly, the total true strain in the y direction was calculated from

$$\varepsilon_y = \ln[(b - l\sin\alpha)/(b - l_0\sin\alpha_0)] \tag{32}$$

We now consider how the fibril length will vary as a function of fibril angle under a change $\Delta\sigma_x$ in an applied tensile stress in the x direction. It has been shown [15] that the change in the moment applied to each fibril in this case is given by

$$\Delta M = -\Delta\sigma_x Y l \sin\alpha/2 \tag{33}$$

where the negative sign indicates that α decreases under a tensile load in the x direction. Substituting Equation 33 into Equation 5 yields

$$\Delta\alpha = -\Delta\sigma_x Y l \sin\alpha/2K_h \tag{34}$$

The change in force applied along the length of each fibril in this case has similarly been shown to be [15]

$$\Delta F = \Delta\sigma_x Y \cos\alpha/2 \tag{35}$$

which when substituted into Equation 8 gives

$$\Delta s = \Delta\sigma_x Y \cos\alpha/2K_s \tag{36}$$

Δs is simply the change in fibril extension, which is therefore also the change Δl in fibril length, i.e.

$$\Delta l = \Delta s \tag{37}$$

In the limit of infinitesimal changes in fibril angle and length Equations 34, 36 and 37 lead to

$$\frac{dl}{d\alpha} = -\frac{K_h}{K_s}\frac{\cot\alpha}{l} = -\frac{lK_h^{eff}}{K_s}\cot\alpha \tag{38}$$

where K_h^{eff} is defined by Equation 29.

In the first instance consider the case of K_s/K_h^{eff} remaining constant. (The transition from elastic to plastic fibril extension can be modelled by K_s/K_h^{eff} adopting a different constant value for the two cases.)

From Equation 38 we have

$$\int_{l_0}^{l} dl/l = -(K_h^{eff}/K_s)\int_{\alpha_0}^{\alpha}\cot\alpha\, d\alpha \tag{39}$$

and hence

$$l = l_0 \exp[(K_h^{eff}/K_s)\ln(\sin\alpha_0/\sin\alpha)] \tag{40}$$

Equation 40 relates the instantaneous value of l to a given value of α during the deformation of the NF microstructure under an applied load in the x direction. The value of α relative to α_0 defines whether the applied load is tensile or compressive and hence Equation 40 is applicable to both loading conditions. Substituting Equation 40 into Equations 31 and 32 gives the total true strains in the x and y directions, respectively, due to a stress applied in the x-direction.

In the case of a y-directed stress it is easily shown that the change in fibril length is related to the change in fibril angle by

$$\frac{dl}{d\alpha} = \frac{lK_h^{eff}}{K_s}\tan\alpha \tag{41}$$

which, assuming K_s/K_h^{eff} remains constant, leads to

$$l = l_0 \exp[(K_h^{eff}/K_s)\ln(\cos\alpha_0/\cos\alpha)] \tag{42}$$

The total true strains in the x and y directions under a y-directed load are, therefore, found by substituting Equation 42 into Equations 31 and 32, respectively.

As an example of how the strain is dependent on the NF model parameters we show, in Fig. 5a, how ε_x varies with α under a stress applied in the x direction for

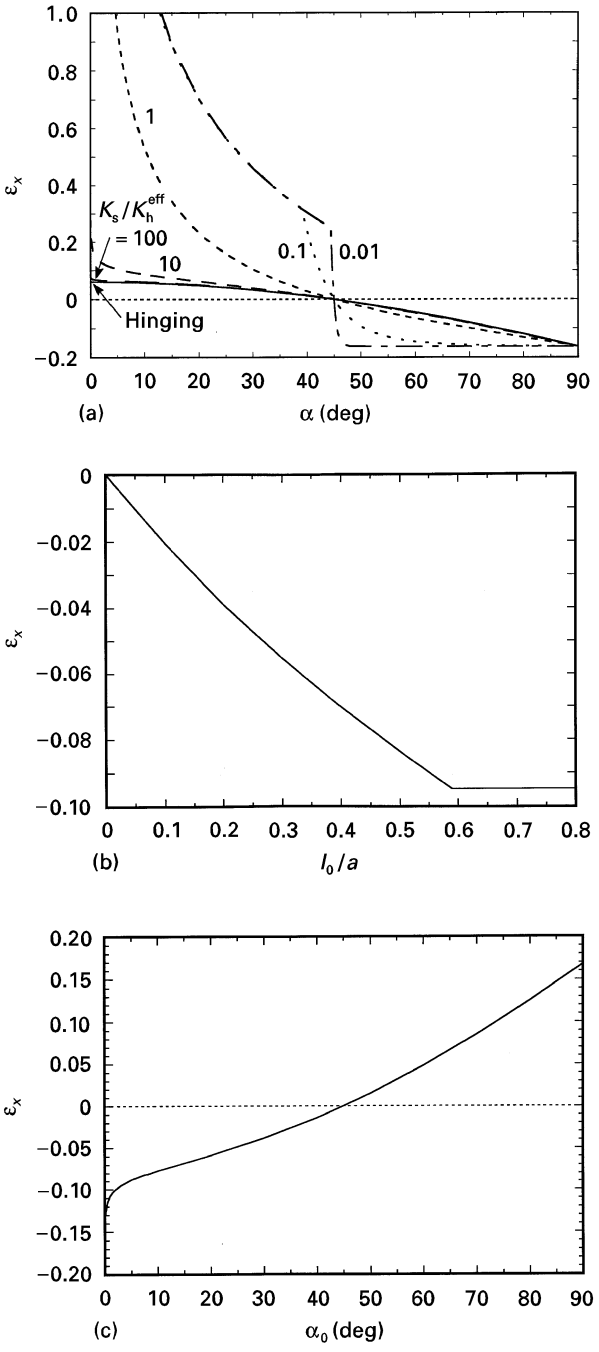

Figure 5 ε_x trends under an x-directed load for the NF model employing concurrent fibril hinging and stretching mechanisms calculated for a standard parameter set of $b/a = 1$, $l_0 = 0.25a$, $\alpha_0 = 45^\circ$, $\alpha = 45^\circ$ and $K_s/K_h^{eff} = 10$. (a) ε_x versus α, with $K_s/K_h^{eff} = 0.01$, 0.1, 1, 10, 100 and ∞ (hinging); (b) ε_x versus l_0/a with $\alpha = 60^\circ$; (c) ε_x versus α_0.

$K_s/K_h^{eff} = 0.01$, 0.1, 1, 10, 100 and ∞ (hinging) with all other parameters as standard. K_s/K_h^{eff} was assumed to remain constant throughout the deformation for each curve.

In Fig. 5a ε_x increases as α decreases from the initial value of $\alpha_0 = 45^\circ$ until a maximum value of $\varepsilon_x = 0.0604$ is achieved at $\alpha = 0^0$ for deformation due to fibril hinging only. The positive value of ε_x indicates that a tensile stress has been applied in the x direction in this case. Conversely, ε_x is negative (i.e. contractile) for $\alpha_0 < \alpha \leqslant 90^\circ$, with the magnitude of ε_x increasing as α increases. The introduction of fibril stretching into the model (i.e. K_s/K_h^{eff} finite) yields an infinite value of ε_x at $\alpha = 0^\circ$. The effect of fibril stretching on ε_x is to increase the magnitude of ε_x at any given value of α, i.e. the larger the value of K_s/K_h^{eff} the closer the ε_x versus α curve is to the hinging only curve.

For $K_s/K_h^{eff} < 1$, stretching dominates and it is necessary to consider the geometrical constraints of the NF network. When the fibril length extends to $l > b/2$ then at some critical angle α_c the nodules will be in contact in the y direction (see Fig. 1c). α_c is given by

$$\sin \alpha_c = b/2l \tag{43}$$

For $K_s/K_h^{eff} \geqslant 1$ further deformation under a tensile load in the x direction (α decreasing) is possible since hinging dominates. However, for a tensile load in the x direction with $K_s/K_h^{eff} < 1$, stretching dominates and values of $\alpha < \alpha_c$ result in nodule overlap in the y direction or the fibrils become slack whilst the nodules remain in contact in the y direction. The former situation is unphysical for a two-dimensional model, and so only the latter is considered here. Hence when Equation 43 was satisfied for $K_s/K_h^{eff} < 1$ the value of l employed in the calculation of ε_x for $\alpha < \alpha_c$ was given by

$$l = b/2 \sin \alpha \tag{44}$$

where l and α now represent the straight line, and the angle, connecting the corners of the nodules to which the slack fibril is connected. For $K_s/K_h^{eff} = 0.1$ and 0.01 Equation 43 is satisfied by $\alpha_c = 39.05$ and 44.40°, respectively. Hence for $\alpha < 39.05^\circ$ the ε_x versus α curves for $K_s/K_h^{eff} = 0.1$ and 0.01 are identical, with the deformation now governed purely by the geometry and arrangement of the nodules. In this new region of deformation behaviour the value of ε_y will remain constant (since the nodules remain in contact in the y direction) with the value given by substituting Equation 43 into Equation 32. Hence $\nu_{xy} = 0$ for $\alpha < \alpha_c$ when $K_s/K_h^{eff} < 1$.

Fig. 5b shows how ε_x varies with l_0 for $\alpha = 60^\circ$ under an x-directed load. All other parameters are as standard. At $\alpha = 60^\circ$, ε_x is contractile (for $\alpha_0 = 45^\circ$), with the magnitude of ε_x increasing with l_0 until $l_0 = 0.5892a$. For $l_0 > 0.5892a$, ε_x remains constant due to the fibrils being slack (i.e. l is given by Equation 44 for $l_0 \geqslant 0.5892a$ and $\alpha = 60^\circ$).

The behaviour of ε_x under a stress in the x direction with α_0 varying is shown in Fig. 5c, with all other parameters as standard. For $\alpha_0 > \alpha\,(= 45^\circ)$ ε_x is positive with the magnitude increasing with α_0, attaining a maximum value of $\varepsilon_x = 0.168$ when $\alpha_0 = 90^\circ$. For $\alpha_0 < \alpha$, ε_x is negative, decreasing to an infinitely negative value as α_0 tends to 0°.

3.3. Fibril angle relaxation at the elastic-to-plastic transition

As already mentioned, the transition from elastic to plastic fibril extension can be modelled by simply reducing the value of K_s/K_h^{eff} at some specified NF network (or fibril) transition strain. Consider a load applied in the x direction which results in the transition from elastic to plastic fibril extension at the transition strain ε_x^T. Substituting Equation 40 into

Equation 31 and rearranging we have

$$\cos\alpha \exp[(K_h^{eff}/K_s)\ln(\sin\alpha_0/\sin\alpha)] = [(a + l_0\cos\alpha_0)\exp(\varepsilon_x^T) - a]/l_0 \quad (45)$$

The right-hand side of Equation 45 is constant at the transition strain, hence as K_s/K_h^{eff} changes for the elastic to plastic value there must be a concommitant change (relaxation) in the fibril angle α. This is easily understood since the stress causing fibril hinging will be dissipated somewhat as the fibril undergoes plastic deformation.

In the case of a y-directed load, substituting Equation 42 into Equation 32 and re-arranging leads to

$$\sin\alpha \exp[(K_h^{eff}/K_s)\ln(\cos\alpha_0/\cos\alpha)] = [b - (b - l_0\sin\alpha_0)\exp(\varepsilon_y^T)]/l_0 \quad (46)$$

where ε_y^T is the transition strain in the y direction. Once again a relaxation of the fibril angle is required for a decrease in K_s/K_h^{eff} at the elastic/plastic transition.

In Fig. 6 we show curves for ν_{xy} versus ε_x calculated using $a = b$, $l_0 = 0.25a$, $\alpha_0 = 90^\circ$ and $K_s/K_h^{eff} = 2$ and 20 when $l \leqslant 1.5l_0$, and $K_s/K_h^{eff} = 0.5$ when $l \geqslant 1.5l_0$, i.e. the elastic to plastic transition occurs when the fibril length has increased by 50% of the initial value. The curves show the same general trends, ν_{xy} becoming increasingly negative (from an initial value of zero at zero strain) as the strain increases, peaking at a strain of $\varepsilon_x \sim l/a$ before decreasing towards $\nu_{xy} \sim 0$ as ε_x increases further. The transition to plastic deformation occurs at $l = 0.375a$ and is seen to result in ν_{xy} flipping from a negative to a positive value which then increases slowly with increasing strain. The effect of decreasing the elastic value of K_s/K_h^{eff} is seen to be a lowering in magnitude of ν_{xy}, a broadening of the ν_{xy} curve and the elastic/plastic transition occurring at a lower value of strain.

3.4. Comparison with experimental data

3.4.1. PTFE

The experimental strain-dependent Poisson's ratio (ν_{xy}) and engineering Young's modulus (E_x^e) data for PTFE [2] are plotted (crosses) against the total true tensile loading strain (ε_x) in Fig. 7a and b, respectively. The PTFE specimen was subjected to a preconditioning process prior to testing which was assumed to leave the sample microstructure in a densified condition. A maximum experimental uncertainty of $\pm 8\%$ is quoted for the Poisson's ratio data [2]. The experimental data for PTFE can be divided into three distinct regions of deformation behaviour [2]. Region I ($0 < \varepsilon_x < 0.15$) is a low Young's modulus region where the deformation is apparently inelastic with a negative Poisson's ratio which increases in magnitude with strain until $\nu_{xy} \sim -11$ at $\varepsilon_x = 0.15$. The deformation is elastic in region II ($0.15 < \varepsilon_x < 0.215$) with the Young's modulus showing a steep increase before achieving a plateau as $\varepsilon_x \to 0.215$. ν_{xy} decreases in magnitude with increasing strain in region II until $\nu_{xy} \sim 0$ at $\varepsilon_x = 0.215$. Plastic deformation is observed in region III ($0.215 < \varepsilon_x < 0.29$) with the Young's modulus showing an extremely steep decrease followed by a tailing off to $E_x^e \sim 0$ at $\varepsilon_x = 0.29$. ν_{xy} adopts

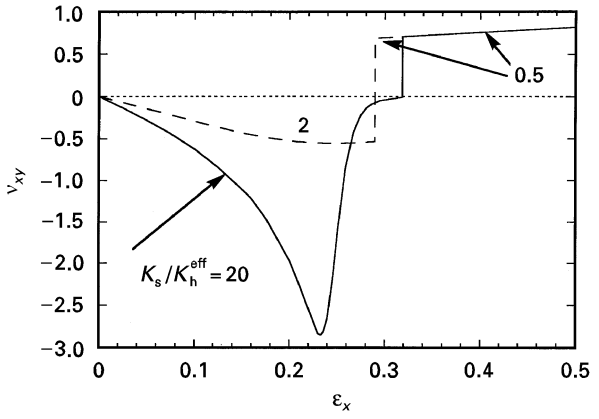

Figure 6 ν_{xy} versus ε_x for the NF model employing concurrent fibril hinging and stretching mechanisms. $b/a = 1$, $l_0 = 0.25a$, $\alpha_0 = 90^\circ$ and $K_s/K_h^{eff} = 2$ and 20 when $l \leqslant 1.5\,l_0$, and $K_s/K_h^{eff} = 0.5$ when $l \geqslant 1.5\,l_0$.

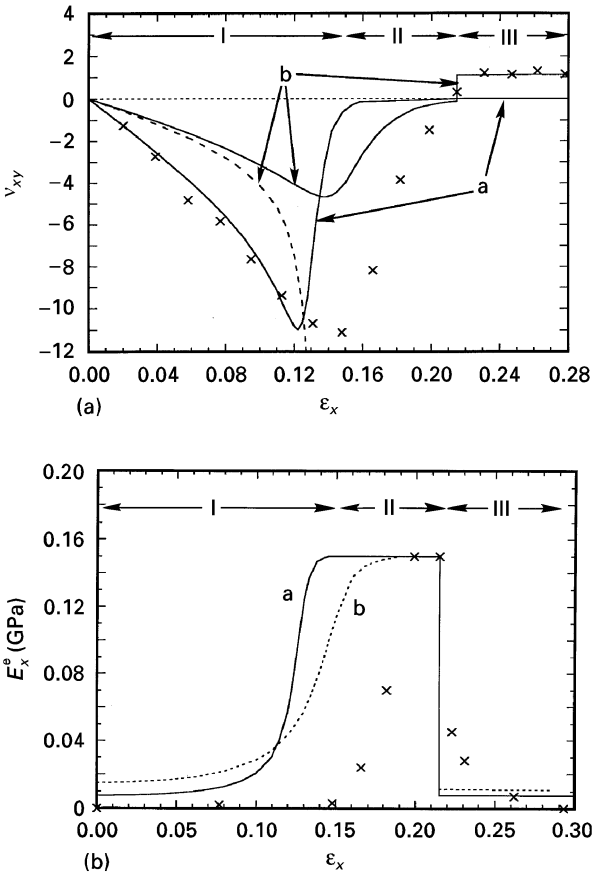

Figure 7 (a) ν_{xy} versus ε_x for the NF model employing fibril hinging (dashed curve) and concurrent fibril hinging and stretching (solid curves) mechanisms. Curves are for: (a) $b = 0.25a$, $l_0 = 0.125a$, $K_s/K_h^{eff} = 20$ (elastic) and $K_s/K_h^{eff} = 1$ (plastic); (b) $b = 0.40a$, $l_0 = 0.14a$, $K_s/K_h^{eff} = 10$ (elastic) and $K_s/K_h^{eff} = 0.65$ (plastic). In all cases $\alpha_0 = 90^\circ$ and K_s/K_h^{eff} is constant at the elastic or plastic value. Transition from elastic to plastic fibril extension was set to occur at $l = 0.24a$. Experimental ν_{xy} data for PTFE [2] are also shown (crosses). (b) E_x^e versus ε_x for the NF model employing concurrent fibril hinging and stretching mechanisms. Model parameters as for Fig. 7(a). Experimental E_x^e data for PTFE [2] are also shown (crosses). Model E_x^e data normalized to peak experimental value of $E_x^e = 0.15$ GPa.

a positive, almost constant, value of $\nu_{xy} \sim 1.2$ throughout region III.

Comparison of the model ν_{xy} versus ε_x curves in Fig. 6 with the experimental data for PTFE in Fig. 7a immediately shows that the model predicts the correct shape and trends for the strain-dependent ν_{xy} data when plastic fibril extension (and concommitant fibril angle relaxation) is assumed to follow elastic fibril extension in the model. In addition to the experimental data we have included NF model calculations in Fig. 7a for: (a) $b = 0.25a$, $l_0 = 0.125a$, $K_s/K_h^{eff} = 20$ (elastic) and $K_s/K_h^{eff} = 1$ (plastic); (b) $b = 0.40a$, $l_0 = 0.14a$, $K_s/K_h^{eff} = 10$ (elastic) and $K_s/K_h^{eff} = 0.65$ (plastic). Calculations for the NF model due to hinging only are also shown (dashed line, same NF dimensions as (b) above). In all cases $\alpha_0 = 90^\circ$ was assumed in accordance with previous experimental and theoretical works [2, 3, 15], and K_s/K_h^{eff} was assumed to remain constant at the elastic or plastic value for the concurrent NF model calculations. The transition from elastic to plastic fibril extension was modelled to occur at $l = 0.24a$ to coincide with the strain at which plastic deformation is observed experimentally.

The nodule and fibril demensions employed in curve (a) were those established in a previous paper [15] and give excellent agreement with the experimental ν_{xy} data for $0 < \varepsilon_x < 0.12$ where hinging is expected to dominate due to the orientation of the fibrils in this strain region. A value of $K_s/K_h^{eff} = 20$ when the fibrils deform elastically reproduces the correct magnitude of ν_{xy} in the concurrent NF model calculations when it is at the maximum negative value (see solid curve (a)). However, this occurs at a strain slightly lower ($\varepsilon_x \sim 0.125$) than that observed experimentally (~ 0.145) with the subsequent decrease in magnitude to $\nu_{xy} \sim 0$ also occurring too swiftly in the model. Increasing the degree of elastic fibril stretching by using a lower K_s/K_h^{eff} value would lead to a small (though insufficient) increase in the strain at which the maximum negative value of ν_{xy} occurs. However, as illustrated in Fig. 6, this would be achieved at the expense of a reduction in the magnitude of ν_{xy}. The value of $l_0 = 0.125a\,(= b/2)$ restricts the possible value of K_s/K_h^{eff} to be employed in the plastic fibril deformation phase to $K_s/K_h^{eff} \geqslant 1$ since the nodules would either overlap (not physical in a 2D model) or the fibrils would become slack (not observed experimentally) otherwise. Hence a positive ν_{xy} is not possible with these constraints for the nodule and fibril dimensions employed in the concurrent NF model calculations for curve (a), the best that can be achieved is $\nu_{xy} = 0$ when $K_s/K_h^{eff} = 1$ ($\varepsilon_x \geqslant 0.215$).

The strain at which the maximum negative value of ν_{xy} occurs in the concurrent NF model is governed to a large extent by the choice of the initial fibril length l_0. Hence a better overall agreement of the ν_{xy} behaviour with strain may be achieved by using an initial value of $l_0 = 0.14a$. Furthermore, to produce a positive ν_{xy} in the plastic fibril stretching phase of the concurrent NF model a value of $b > 2l_0$ is required when $\alpha_0 = 90^\circ$. The hinging and concurrent NF model calculations for $b = 0.4a$, $l_0 = 0.14a$ and $\alpha_0 = 90^\circ$ are shown as curves (b) in Fig. 7a. These parameters (with $K_s/K_h^{eff} = 10$ in the elastic fibril stretching stage) do indeed predict the correct strain at which the maximum negative ν_{xy} occurs. However, the magnitude of ν_{xy} during the elastic fibril stretching phase is consistently underestimated in these calculations. $K_s/K_h^{eff} > 10$ would improve the agreement with experiment for $0 < \varepsilon_x < 0.14$. However, the hinging only (i.e. $K_s/K_h^{eff} = \infty$) model calculations (dashed curve (b)) give the maximum negative ν_{xy} value at any given value of α for these nodule and fibril dimensions, and hence complete agreement with the experimental data will not be achieved. This combination of nodule and fibril dimensions does, however, allow a value of $K_s/K_h^{eff} < 1$ to be employed in the plastic fibril extension phase, and in this case $K_s/K_h^{eff} = 0.65$ in seen to reproduce the experimental ν_{xy} data very well in the strain range $0.215 < \varepsilon_x < 0.29$.

The calculated concurrent NF model E_x^e versus ε_x curves in Fig. 7b show the same trends to the experimental data. The model curves are for the same parameters as used for the curves in Fig. 7a. All the model E_x^e data were normalized to the maximum experimental data peak of $E_x^e = 0.15$ GPa. However, the model curves overestimate E_x^e in the lower strain region and reach the maximum value at an earlier strain than the experimental data. Curve (a) increases to a maximum value earlier than curve (b) due to the lower initial fibril length employed in the calculations for curve (a).

3.4.2. UHMWPE

The experimental strain-dependent Poisson's ratio (ν_{yx}) versus total true compressive strain in the loading (y) direction ($\varepsilon_y^c = -\varepsilon_y$) data for UHMWPE [12, 16] are presented in Fig. 8 (crosses). Two regions of deformation behaviour are observed: region I ($\varepsilon_y^c < 0.037$) has a small negative ν_{yx} at low strains which increases slowly with increasing strain until a large increase in magnitude to $\nu_{yx} \sim -15$ is observed at the highest strains; region II ($\varepsilon_y^c > 0.037$) is a region of positive or

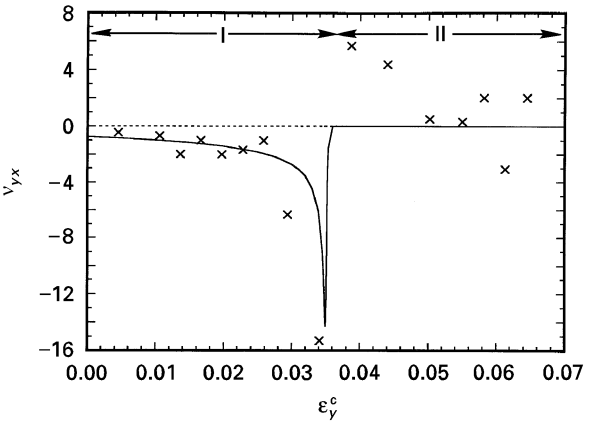

Figure 8 ν_{yx} versus $\varepsilon_y^c (= -\varepsilon_y)$ for the NF model employing concurrent fibril hinging and stretching mechanisms (solid curve). Calculations are for $b = a$, $l_0 = 0.09a$ and $\alpha_0 = 40^\circ$. $K_s/K_h^{eff} = 1000$ throughout. Experimental ν_{yx} data for UHMWPE [12, 16] are also shown (crosses).

zero ν_{yx}. The transition from large negative to positive ν_{yx} occurs rapidly at the transition from region I to region II ($\varepsilon_y^c \sim 0.037$). No Young's modulus data exist for this UHMWPE data set. Due to the stiffness of the auxetic UHMWPE sample no preconditioning process was necessary prior to testing. Hence, the value of α_0 was not constrained to be either 90 or 0°.

In an earlier paper [15] the ν_{yx} data for UHMWPE were found to be reasonably well reproduced by the NF model, assuming hinging occurs prior to fibril stretching for nodule and fibril dimensions of $a = b$, $l_0 = 0.095a$ and $\alpha_0 = 40°$. The concurrent NF model curve, calculated using Equations 23 and 32, for $a = b$, $l_0 = 0.09a$, $\alpha_0 = 40°$ and $K_s/K_h^{eff} = 1000$ is also shown in Fig. 8 (the slightly lower value of l_0 to that used previously was chosen to allow for some stretching occurring during the predominantly hinging phase of the concurrent model calculations). The model is seen to predict the overall strain-dependent behaviour of the experimental ν_{yx} data very well. The high value of K_s/K_h^{eff} employed in the calculations ensures that the transition from region I to region II is suitably abrupt whilst allowing the model to predict the correct magnitude of ν_{yx} immediately prior to the transition. It is to be noted, however, that the model calculations presented in Fig. 8 do not predict a positive ν_{yx} in region II. However, no transition from elastic to plastic fibril extension has been included here. This will be discussed in Section 4.2.

4. Discussion

In this paper the strain-dependent deformations of auxetic microporous PTFE and UHMWPE have been found to be reproduced remarkably well by a NF model incorporating concurrent fibril hinging and stretching deformation mechanisms when the ratio of the force coefficients governing the two mechanisms is assumed to have a constant value during either elastic or plastic fibril extension. However, some discrepancies do still exist between the data and the model calculations. These are discussed in this section.

4.1. PTFE

In Fig. 7a the correct shape of the ν_{xy} versus ε_x data was predicted by the model. However, different combinations of nodule and fibril dimensions and force coefficients were required to reproduce the correct strain scaling and magnitude of ν_{xy} when at its maximum negative or positive values. The calculations with $b = 0.25a$, $l_0 = 0.125a$ and $K_s/K_h^{eff} = 20$ (solid curve (a)) were found to be in excellent agreement with experiment for $\varepsilon_x < 0.12$ and also predicted the correct maximum negative value of $\nu_{xy} \sim -11$. However, the agreement deteriorated for $\varepsilon_x > 0.12$ and it was found to be impossible to predict a positive ν_{xy} at the higher strains due to the constraints placed on the possible values of K_s/K_h^{eff} to be employed for plastic fibril deformation by the nodule-fibril geometry. Increasing both b/a and l_0 allowed greater agreement in the strain at which the maximum negative ν_{xy} occurs and the magnitude of the maximum positive ν_{xy} (during plastic fibril deformation) to be achieved. However, this was at the cost of decreasing the agreement at the lower strains in the magnitude of the negative ν_{xy} values.

Several effects may help to explain these discrepancies. In particular the model assumes: (i) a constant force coefficient ratio during elastic or plastic fibril extension; (ii) the nodules are square or rectangular in shape; (iii) the nodule–fibril network is two-dimensional; (iv) the nodules do not deform during deformation of the network.

The assumption of constant K_s/K_h^{eff} during elastic or plastic fibril extension is unlikely to be valid. Equation 38 reveals that a knowledge of the force coefficients is required in order to calculate the fibril length as a function of fibril angle. The stretching force coefficient has been shown [15] to take the form

$$K_s = E_s wt/l \tag{47}$$

for a fibril of length l, thickness t, depth w and Young's modulus E_s. From Equations 29 and 47 we have

$$K_s/K_h^{eff} = E_s V/K_h \tag{48}$$

where V is the fibril volume ($V = wtl$). Hence K_s/K_h^{eff} is dependent on three variables: E_s, V and K_h.

The form of K_h to be employed in the calculations for PTFE and UHMWPE is likely to be complicated [15], the physical origin being either due to friction forces acting between nodules [2] or due to shearing and polymer chain alignment effects in the material connecting the fibrils to the nodules.

Furthermore, the mechanisms of fibril extension may involve processes other than simple elastic or plastic extension of the original fibril material (e.g. drawing out of the hinge material into fibril material may occur as the applied stress increases). Even in the case of the original fibril material deforming elastically, the deformation may not be linear and hence E_s may also vary with deformation. The fibril volume will increase as the deformation proceeds, due to the usual increase associated with a stretched elastic material and also any new fibril material created due to drawing out of the hinge material. A treatment where fibril volume effects due to elastic stretching are taken into account is given in the Appendix. However, the value of l due to volume changes in this case is equal to within $< 4\%$ of that obtained when V is assumed constant for extensions of l up to 50% in the calculations with $K_s/K_h^{eff} = 10$ initially and an intrinsic fibril Poisson's ratio of $\nu_s \sim 0.20$ (typical value for the polymers considered in this paper) – see Appendix. Nevertheless, Equation 48 indicates that the behaviour of K_s/K_h^{eff} with deformation is likely to be exceedingly complex.

It is instructive, therefore, to consider the strain-dependent ν_{xy} behaviour for K_s/K_h^{eff} allowed to vary during the deformation. Plots of ε_y versus ε_x are presented in Fig. 9, calculated using the concurrent NF model for the PTFE geometrical parameters of $b = 0.25a$, $l_0 = 0.125a$, $\alpha_0 = 90°$ with $K_s/K_h^{eff} = 200$, 20, 10 and 5. From the definition of Poisson's ratio (Equation 11), ν_{xy} is simply the negative of the slope in Fig. 9. For $\varepsilon_x \leqslant 0.10$ the curves for $K_s/K_h^{eff} = 200$, 20 and 10

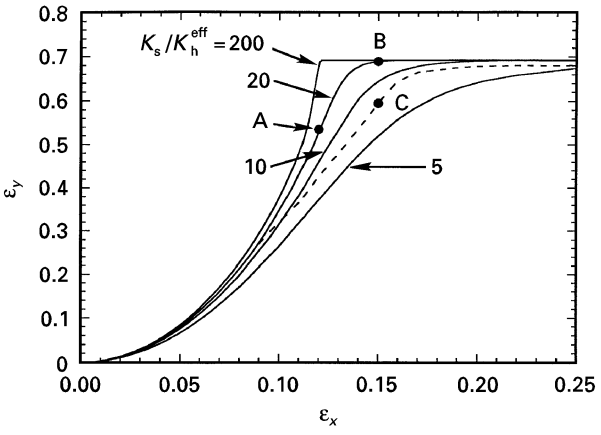

Figure 9 ε_y versus ε_x for the NF model employing concurrent fibril hinging and stretching mechanisms under an x directed load. Calculations are for $b = 0.25a$, $l_0 = 0.125a$, $\alpha_0 = 90^\circ$ and $K_s/K_h^{eff} = 200$, 20, 10 and 5. Dashed curve corresponds to K_s/K_h^{eff} arbitrarily decreasing from $K_s/K_h^{eff} = 20$ as ε_x increases from $\varepsilon_x \sim 0.10$

almost coincide, indicating that any variation in the force coefficient ratio in this range of values would probably be beyond the limits of experimental observation. In other words, the assumption of a constant K_s/K_h^{eff} value is not critical in this strain region. However, for $\varepsilon_x > 0.10$ the curves diverge sufficiently for the constant force coefficient ratio assumption to become questionable.

Consider the curve for $K_s/K_h^{eff} = 20$. At $\varepsilon_x \sim 0.12$ (point A) the slope of the curve gives a value of ν_{xy} close to the maximum negative value observed experimentally (see also Fig. 7a). However, experimentally this value of ν_{xy} occurs at a strain of $\varepsilon_x \sim 0.15$, whereas the slope of the ε_y versus ε_x curve in Fig. 9 for $K_s/K_h^{eff} = 20$ at $\varepsilon_x \sim 0.15$ (point B) yields $\nu_{xy} \sim 0$. By allowing K_s/K_h^{eff} to vary throughout the deformation much closer agreement can be achieved. For example, in Fig. 9 we also show a curve for K_s/K_h^{eff} allowed to vary between 20 and 5, with the value decreasing as strain increases above $\varepsilon_x \sim 0.10$ (dashed curve). The slope of the dashed curve at $\varepsilon_x \sim 0.15$ (point C) now gives a much larger negative value of ν_{xy} than the $K_s/K_h^{eff} = 20$ curve at the same strain ($\nu_{xy} \sim 0$), with the slope (and, therefore, ν_{xy}) similar to that at $\varepsilon_x \sim 0.12$ for the $K_s/K_h^{eff} = 20$ curve (point A).

Hence the model ν_{xy} versus ε_x data in Fig. 7a for $b = 0.25a$, $l_0 = 0.125a$ and $K_s/K_h^{eff} = 20$ (solid curve (a)) would show improved agreement with the experimental data for $\varepsilon_x > 0.12$ if K_s/K_h^{eff} was allowed to decrease with increasing strain.

Allowing K_s/K_h^{eff} to vary could also produce a positive ν_{xy} if the rate of change of K_s/K_h^{eff} with strain was sufficiently large to change the sign of the slope of the dashed line in Fig. 9. This will be considered in Section 4.2 for UHMWPE. However, the experimental Young's modulus data for PTFE suggest a much more abrupt change in K_s/K_h^{eff} occurs at $\varepsilon_x \sim 0.215$ (see Fig. 7b) corresponding to the onset of plastic deformation.

Improved agreement in the higher strain elastic data ($0.12 < \varepsilon_x < 0.215$) could also be achieved by the second effect to be considered, namely, nodule shape. In the real materials the nodules are observed to be approximately circular or elliptical in shape. A rigorous NF model with elliptical nodules is not attempted here. However, for circular or elliptical nodules, where the fibrils are assumed to be capable of "wrapping" round the nodules, then as the network is subjected to a tensile stress in the x direction the network will expand and the fibrils will "unwrap" with the result that the effective b/a ratio and the active fibril length (the "unwrapped" length) will also increase. In Fig. 7a the nodule shape effect would tend, therefore, to increase the values of b/a and l_0 to be used in the model calculations as the strain increases. In other words since the curve for $b/a = 0.25$ and $l_0 = 0.125a$ (solid curve (a)) is a good fit to the lower strain experimental data, a better fit to the higher strain data would be expected from considerations of nodule shape for a larger value of b/a and l_0. This is indeed observed for curve (b) when $\varepsilon_x > 0.135$ in Fig. 7a.

The assumption of a 2D node-fibril network in the NF model has consequences on both the apparent fibril extension in the inelastic stage (region I) of deformation and the apparent lower limit on the force coefficient ratio during the plastic stage (region III) of deformation for auxetic PTFE (see Fig. 7).

For the geometrical parameters of $b/a = 0.25$, $l_0 = 0.125a$ and $\alpha_0 = 90^\circ$, known to give a good fit to the low strain data ($\varepsilon_x < 0.12$) for PTFE, the fibril length used in the NF model must be approximately double its initial length [15] at the region I-to-region II transition. One reason for the apparently inelastic increase in length during region I is thought to be due to drawing out of fibril material from the ('hinge') material connecting the fibril to the nodule. However, an additional contribution may also be found by considering a 3D node–fibril network, as observed in reality. As a tensile stress is applied in the x direction the fibrils will become aligned in the x–y plane such that the length of the projection of the fibrils in this plane will increase as ε_x increases. In other words, the fibril length used in the 2D model will in fact be a projection in the x–y plane of the length of the fibril in the real material. 'Extension' of the fibril in the model will, therefore, have components corresponding to both actual fibril extension and fibril alignment effects.

We have already seen that if the fibrils are to remain taut then the assumption of a 2D model places a lower limit on K_s/K_h^{eff} due to the nodules being unable to overlap. However, in a 3D material nodule overlap will be possible, depending on the connectivity of the nodules in the z direction. Hence, for example, a value of $K_s/K_h^{eff} < 1$ may be used in the calculations for plastic deformation of PTFE when $b/a = 0.25$, $l_0 = 0.125a$ and $\alpha_0 = 90^\circ$, leading to a positive value of ν_{xy} for these parameters in Fig. 7a, as opposed to the limiting value of $\nu_{xy} = 0$ in the 2D case.

The fourth effect of nodule deformation is not considered here, since there is no published data to indicate this mechanism occurs in either the PTFE or UHMWPE samples considered in this paper. We simply state that nodule deformation could be a cause for the discrepancy between the NF model and experiment.

It is clear, however, that the ν_{xy} data for auxetic PTFE can be understood in terms of concurrent fibril hinging and stretching mechanisms acting in a nodule–fibril network.

Allowing for the above effects will also be expected to improve the agreement between the model and experimental E_x^e data for PTFE presented in Fig. 7b. However, an additional complication needs to be taken into account for the E_x^e data. The model calculations for E_x^e in Fig. 7b assume not only a constant K_s/K_h^{eff} ratio during elastic or plastic fibril extension, but also that K_s and K_h^{eff} each remain constant. This is a more restrictive constraint than K_s/K_h^{eff} remaining constant since K_s/K_h^{eff} could remain constant if K_s and K_h^{eff} were correlated but not necessarily constant themselves. There is evidence that in the initial stages of fibril extension the length of the fibrils increases predominantly due to drawing out of the material connecting the fibrils to the nodules into fibrillar material. This would have the effect of lowering the value of K_s compared to that with purely elastic fibril extension and, since E_x^e depends on the actual values of K_s and K_h^{eff} rather than the ratio (see Equation 17), would therefore account for the model calculations overestimating E_x^e at low strain in Fig. 7b.

It is, however, extremely gratifying that the predicted ν_{xy} and E_x^e trends from the NF model are entirely consistent with the experimental data for PTFE; the Young's modulus data confirming the mechanisms used to predict the Poisson's ratio data appear to have been correctly identified.

4.2. UHMWPE

In the model calculations used to predict the ν_{yx} versus ε_y^c behaviour of UHMWPE (Fig. 8) no attempt was taken to model the possiblity of the fibrils undergoing a transition from elastic to plastic extension. The reason being that, unlike PTFE where the deformation is over a large total strain range of $0 \leqslant \varepsilon_x \leqslant 0.29$, the total strain range covered experimentally during the deformation of the UHMWPE sample was relatively low at $0 \leqslant \varepsilon_y^c \leqslant 0.065$. Hence a sudden step transition from elastic to plastic deformation at a clearly defined strain is unlikely to be an appropriate approximation in the UHMWPE case. This is demonstrated by examining the experimental PTFE data (Fig. 7a and b) where it is clear that the transition from elastic to plastic deformation occurs over the strain range $0.215 < \varepsilon_x < 0.23$, i.e. a change in strain of 0.015. This represents $\sim 5\%$ of the total strain range covered for PTFE and can, therefore, be reasonably represented as a sudden transition from elastic to plastic deformation. In the case of UHMWPE a similar transition strain range of 0.015 for the transition from elastic to plastic deformation represents $\sim 23\%$ of the total strain range covered experimentally and hence a discrete transition strain is not appropriate in the model.

In fact, if we consider the onset of the transition strain range in UHMWPE occurs at $\varepsilon_y^c \sim 0.036$ (see Fig. 8), then a transition strain range of 0.015 implies that the end of the transition strain range occurs at $\varepsilon_y^c \sim 0.051$. This range of strain coincides exactly with the positive values of ν_{yx} ($0 < \nu_{yx} < +6$) observed in the experimental data. The uncertainties associated with the experimental ν_{yx} data in this region are ± 1 (estimated from three different methods of analysis of the raw experimental strain data [16]), indicating that these positive values (so far unexplained by the model) are genuine. As already indicated a NF model where the force coefficients ratio is allowed to vary smoothly with strain is beyond the scope of this paper. However, the effects of varying K_s/K_h^{eff} over a finite range of strain will again be considered quantitatively.

In Fig. 10 we plot the transverse contractile strain ($\varepsilon_x^c = -\varepsilon_x$) versus the compressive strain in the loading direction (ε_y^c) for the NF model calculations with $a = b$, $\alpha_0 = 40^\circ$, $l_0 = 0.09a$ and $K_s/K_h^{eff} = 1000$, 100, 20, 10, 5 and 2. These calculations are for the same nodule and fibril dimensions used in Fig. 8 to explain the experimental UHMWPE ν_{yx} data, which used a value of $K_s/K_h^{eff} = 1000$. The strain-dependent NF model ν_{yx} is in fact given by the negative of the tangent to the strain–strain curve at any point on the curve in Fig. 10. Hence if a value of $K_s/K_h^{eff} = 1000$ is assumed throughout, the slope of the curve in Fig. 10 results in a negative ν_{yx} increasing in magnitude with strain until $\varepsilon_y^c \sim 0.036$, whereupon a relatively sudden change to $\nu_{yx} \sim 0$ is observed for all strains thereafter (i.e. the model ν_{yx} curve in Fig. 8). However, if a transition from elastic to plastic fibril extension was to occur over the range $0.036 < \varepsilon_y^c < 0.051$ corresponding to a change in K_s/K_h^{eff} from 1000 to 2, then the value of ε_x^c would decrease as ε_y^c increases above 0.036. This is indicated by the dashed line in Fig. 10. The slope of the dashed curve in Fig. 10 results in a positive value of ν_{yx}, as observed experimentally. Above $\varepsilon_y^c \sim 0.05$ the deformation would then proceed according to the curve corresponding to the plastic value of K_s/K_h^{eff}, e.g. $K_s/K_h^{eff} = 2$ in Fig. 10, which results in $\nu_{yx} \sim 0$ due to the relatively flat nature of this curve. The strain–strain behaviour described above due to K_s/K_h^{eff} decreasing from an elastic to plastic value over a finite strain range explains, therefore, the ν_{yx} behaviour observed experimentally and in

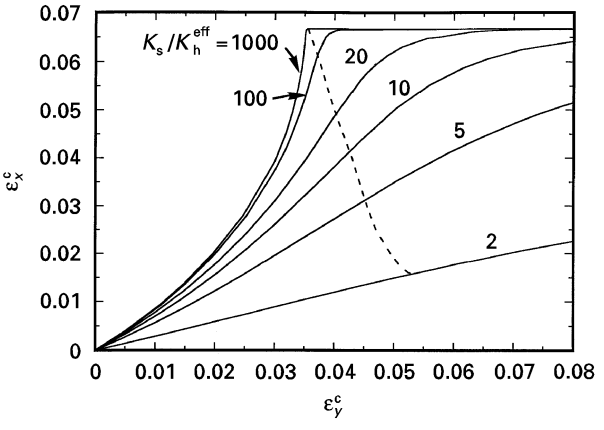

Figure 10 ε_x^C versus ε_y^C for the NF model employing concurrent fibril hinging and stretching mechanisms under a y directed load. Calculations are for $b = a$, $l_0 = 0.09a$, $\alpha_0 = 40^\circ$ and $K_s/K_h^{eff} = 1000$, 100, 20, 10, 5 and 2. The dashed curve illustrates the effect of decreasing K_s/K_h^{eff} from 1000 to 2 in the strain range $0.036 < \varepsilon_y^C < 0.05$.

fact corresponds to the ε_x^c versus ε_y^c trends observed experimentally [12, 16].

In an earlier paper [15] it was suggested that the positive ν_{yx} values observed experimentally may arise as a result of nodule interactions due to non-rectangular nodule shapes. However, preliminary investigations show that it is unlikely that values as large as $\nu_{yx} = +6$ would be achieved due to a nodule shape effect, which may in any event not occur due to nodule overlap being possible for a 3D material. Furthermore, the range of strain required for the nodule interactions to show the tailing off to $\nu_{yx} \sim 0$ at the highest strains appears to be an order of magnitude higher than that observed in UHMWPE. Hence, the transition from elastic to plastic fibril extension over a finite range of strain seems the more likely scenario.

Fig. 10 also illustrates that for $\varepsilon_y^c < 0.02$ the value of K_s/K_h^{eff} can decrease from 1000 by almost two orders of magnitude without significantly affecting the Poisson's ratio. Again, it is unlikely that experimental measurements on the strain data would be sensitive to detecting such a change in K_s/K_h^{eff} in this strain range. Hence the assumption of a constant K_s/K_h^{eff} in this region of strain is not critical.

5. Conclusions

The experimental strain-dependent deformations of auxetic microporous PTFE and UHMWPE can be explained entirely in terms of a NF model employing concurrent fibril hinging and stretching deformation mechanisms. In this paper the deformation of a network of rigid rectangular nodules interconnected by fibrils has been assumed to occur with a constant force coefficient ratio governing the two mechanisms. The dependence of the Poisson's ratios and Young's moduli on the model parameters have been investigated. The force coefficient ratio is a function of, amongst other properties, the intrinsic Young's modulus of the fibrils themselves and so a different value has been used for the fibrils deforming elastically and plastically. The overall trends of the experimental data for both polymers are predicted by the model. However, absolute agreement requires a knowledge of the nodule shape, how the force coefficient ratio varies with strain and how the nodules are connected into a 3D network. These effects have been discussed, but no rigorous treatment has been presented here.

Appendix Effect of fibril volume variation on calculation of fibril length

The expression relating the fibril length to the fibril angle at any instant in the deformation of the NF network is derived here for the case of constant K_h and E_s, with fibril volume, V, varying according to linear elasticity theory.

For linear elastic behaviour the fibril Poisson's ratio ν_s is defined by the ratio of the total true strains

$$\nu_s = -\varepsilon_T/\varepsilon_L \tag{A1}$$

where ε_T and ε_L are the transverse and longitudinal fibril strains, respectively, due to a stress applied longitudinally. Consider the linear deformation of a fibril of initial length l_0 and transverse thickness t_0 to a deformed length and thickness of l and t, respectively, due to a stress applied along the fibril length. By analogy with Equation 30, Equation A1 becomes

$$\nu_s = -\ln(t/t_0)/\ln(l/l_0) \tag{A2}$$

Provided the deformation is linear, Equation A2 is valid for all strain, whereas similar expressions using total engineering strains are always approximations to ν_s and fail significantly at large strains. Rearranging Equation A2 yields

$$(l_0/l)^{\nu_s} = (t/t_0) \tag{A3}$$

For a fibril of equal thickness and depth the deformed (V) to undeformed (V_0) volume ratio is simply

$$(V/V_0) = (l/l_0)(t/t_0)^2 \tag{A4}$$

From Equations A3 and A4

$$(V/V_0) = (l/l_0)^{(1-2\nu_s)} \tag{A5}$$

and hence the variation in fibril volume is determined entirely by the fibril length and fibril Poisson's ratio in this case. Note that when $\nu_s = 1/2$ the volume remains constant, as required by elasticity theory.

Substituting Equations A5 and 48 into Equation 38 we find, for an x-directed load, the change in fibril length is related to the change in fibril angle by

$$\frac{dl}{d\alpha} = -\frac{K_h}{E_s V_0}\frac{l_0^{(1-2\nu_s)}}{l^{(-2\nu_s)}}\cot\alpha \tag{A6}$$

Following the procedure outlined in Section 3.2, Equation A6 integrates to

$$l = l_0[(2\nu_s - 1)(K_h/E_s V_0)\ln(\sin\alpha/\sin\alpha_0) + 1]^{[1/(1-2\nu_s)]} \tag{A7}$$

which is the equation relating the fibril length to the fibril angle in the concurrent NF model under an x-directed load when fibril volume effects are considered due to linear elastic behaviour only, with K_h and E_s assumed constant.

It is readily shown that the equivalent to Equation A7 for a y-directed load is

$$l = l_0[(2\nu_s - 1)(K_h/E_s V_0)\ln(\cos\alpha/\cos\alpha_0) + 1]^{[1/(1-2\nu_s)]} \tag{A8}$$

To gain a feel for the effect of fibril volume variations we calculate l/l_0 for constant fibril volume (Equation 40) with $K_s/K_h^{eff} = 10$ and for fibril volume varying elastically (Equation A7) with $E_s V_0/K_h = 10$ (i.e. same initial force coefficients ratio in the two cases – see Equation 48) under a tensile x-directed load from an undeformed fibril angle of $\alpha_0 = 90^\circ$. A typical value for polymers of $\nu_s = 0.2$ was used in Equation A7. At $\alpha = 20^\circ$, $l/l_0 = 1.1133$ and 1.1096 for the constant and variable volume conditions, respectively, i.e. the discrepancy in $l \sim 0.3\%$ when l has increased by $\sim 10\%$. When $\alpha = 5^\circ$, $l/l_0 = 1.2764$ and 1.2557 for constant and variable volume, respectively (discrepancy $\sim 1.6\%$). At $\alpha = 1^\circ$, $l/l_0 = 1.4990$ and 1.4368 for constant and variable volume, respectively, i.e. when the

fibril has stretched by $\sim 50\%$ the discrepancy between the two equations is only 4% for the values used in these calculations. Hence in this case the effect of fibril volume on the length of the fibrils is negligible in the range $1 \leqslant \alpha \leqslant 90^{\circ}$.

Acknowledgements

The authors acknowledge the support of the Engineering and Physical Sciences Research Council of the United Kingdom. KEE wishes to acknowledge the award of an EPSRC Advanced Fellowship during this work.

References

1. K. E. EVANS, M. A. NKANSAH, I. J. HUTCHINSON and S. C. ROGERS, *Nature* **353** (1991) 124.
2. B. D. CADDOCK and K. E. EVANS, *J. Phys. D*: *Appl. Phys.* **22** (1989) 1877.
3. K. E. EVANS and B. D. CADDOCK, *ibid.* **22** (1989) 1883.
4. K. L. ALDERSON and K. E. EVANS, *Polymer* **33** (1992) 4435.
5. R. LAKES, *Science* **235** (1987) 1038.
6. K. E. EVANS, M. A. NKANSAH and I. J. HUTCHINSON, *Acta Metall. et Mater.* **42** (1994) 1289.
7. A. YEGANEH-HAERI, D. J. WEIDNER and J. B. PARISE, *Science* **257** (1992) 650.
8. N. R. KESKAR and J. R. CHELIKOWSKY, *Nature* **358** (1992) 222.
9. K. E. EVANS, *Endeavour* **15** (1991) 170.
10. K. L. ALDERSON, A. P. PICKLES, P. J. NEALE and K. E. EVANS, *Acta Metall. et Mater.* **42** (1994) 2261.
11. K. L. ALDERSON and K. E. EVANS, *J. Mater. Sci.* **28** (1993) 4092.
12. P. J. NEALE, K. L. ALDERSON, A. P. PICKLES and K. E. EVANS, *J. Mater. Sci. Lett.* **12** (1993) 1529.
13. A. P. PICKLES, K. L. ALDERSON and K. E. EVANS, *Polym. Eng. & Sci.* **36** (1996) 636.
14. K. E. EVANS, *J. Phys. D*: *Appl. Phys.* **22** (1989) 1870.
15. A. ALDERSON and K. E. EVANS *J. Mater. Sci.* **30** (1995) 3319.
16. K. L. ALDERSON, A. ALDERSON and K. E. EVANS, *J. Strain Analysis for Engineering Design*, submitted.
17. M. F. BEATTY and D. O. STALNAKER, *J. Appl. Mech.* **53** (1986) 807.
18. J. E. SHIGLEY, "Applied Mechanics of Materials" (McGraw-Hill, New York, 1976).
19. B. M. LEMPRIERE, *Amer. Inst. Aeronaut. Astronaut. J.* **6** (1968) 2226.

Received 18 October
and accepted 13 November 1996